

1 **New Inferences on Magma Dynamics in Melilitite-Carbonatite Volcanoes: The Case**
2 **Study of Mt. Vulture (Southern Italy)**

3 **G. Carnevale¹, A. Caracausi², S. G. Rotolo^{1,2}, M. Paternoster^{2,3}, and V. Zanon⁴**

4 ¹ Dipartimento di Scienze della Terra e del Mare, Università degli Studi di Palermo, Palermo,
5 Italy, ² Istituto Nazionale di Geofisica e Vulcanologia, Sezione di Palermo, Palermo, Italy, ³
6 Dipartimento di Scienze, Università degli Studi della Basilicata, Potenza, Italy, ⁴ Instituto de
7 Vulcanologia e Avaliação de Riscos, Universidade dos Açores, Ponta Delgada, Portugal

8 Corresponding author: Gabriele Carnevale (gabriele.carnevale@unipa.it)

9 **Key Points:**

- 10 • Micro-thermometric analyses show the occurrence of high-density CO₂-rich fluid
11 inclusions within wehrlite xenoliths
- 12 • Estimates on magma ascent rate show how a melilitite-carbonatite magma can be
13 comparable with ascent rate of kimberlite magmatism
- 14 • Melilitite-carbonatite volcanoes can be hazardous even after long time of quiescence (>
15 10⁵ years)

16 **Abstract**

17 This study provides the first micro-thermometric data of fluid inclusions in mafic loose
18 xenocrysts and ultramafic xenoliths in explosive products of the melilitite-carbonatite Mt.
19 Vulture volcano (southern Italy). We found within ultramafic xenoliths CO₂-dominated fluid
20 inclusions with trapping pressures between 8.5 and 8.9 kbar, corresponding to a depth of 26-27
21 km, in proximity of the local crust-mantle boundary. In contrast, trapping pressures within the
22 loose xenocrysts are up to 2.8 and 3.2 kbar (8-9 km). We estimated an ascent rate of the latest
23 141 ka old melilititic-carbonatitic magmas from the Moho depth to the surface in the range of
24 few hours. Considering the ongoing degassing of mantle-derived CO₂ rich gases at Mt. Vulture,
25 together with geophysical evidences of the presence of low amount of melts at depth, and the
26 tectonic control of the past volcanic activity, our study opens new perspective about the
27 hazardous nature of the “quiescent” melilitite-carbonatite volcanoes.

28 **Plain Language Summary**

29 The study of fluid inclusions can provide important information about the environments and
30 magmatological processes in which the host minerals formed. Investigating their composition
31 and trapping pressure and temperature it is possible to constrain magma ascent history. To
32 understand the last explosive volcanic activity of Mt. Vulture volcano (southern Italy), we
33 investigated fluid inclusions in mafic minerals, and ultramafic xenoliths brought to the surface by
34 a melilitite-carbonatite magma. Our results show the presence of CO₂-rich fluid inclusions with
35 trapping pressure corresponding to a depth of 26-27 km in ultramafic xenoliths, and a shallower
36 depth (8-9 km) in mafic minerals. Estimates on magma ascent rate show rapid ascent dynamics
37 to the surface (hours). Our study emphasizes the importance of a multidisciplinary approach that
38 combine geophysics, geochemistry and petrology to investigate a volcanic system even if the
39 volcano is considered “quiescent”, as is the case of Mt. Vulture volcano, where currently active
40 magmatic degassing occurs.

41 **1 Introduction**

42 Carbonatite magmatism is mainly associated with intraplate continental tectonic settings, with a
43 temporal distribution from Archean to the present (*e.g.*, Jones et al., 2013; Woolley & Kjarsgaard,
44 2008), and currently, Oldoinyo Lengai (Tanzania) represents the only active carbonatite volcano,
45 characterised by a natrocarbonatitic affinity. The growing number of carbonatite occurrences from
46 unconventional tectonic settings, such as oceanic contexts (*e.g.*, Carnevale et al., 2021; Doucelance
47 et al., 2010; Mata et al., 2010; Schmidt & Weidendorfer, 2018) or subduction zones (*e.g.*, D’Orazio
48 et al., 2007; Li et al., 2018), received considerable attention during last two decades, given their
49 importance as source of rare elements (Verplanck et al., 2019), and, most importantly, because
50 they provide meaningful information about the geochemical cycle of carbon and mantle
51 metasomatism as well (*e.g.*, Bouabdellah et al., 2010; Horton, 2021).

52 Mt. Vulture (southern Italy) is an isolated volcano located between the Apulia foreland and the
53 eastern side of the Apennine orogenic belt, within the particular geodynamic context of the
54 Apennine subduction zone (D’Orazio et al., 2007; Peccerillo, 2017). This volcano is located along
55 the deep NE-SW lithospheric faults that represent the tear of the slab, a potential pathway for the

56 ascent of magmatic bodies and mantle derived fluids (Caracausi et al., 2013a; D’Orazio et al.,
57 2007; Rosenbaum et al., 2008).

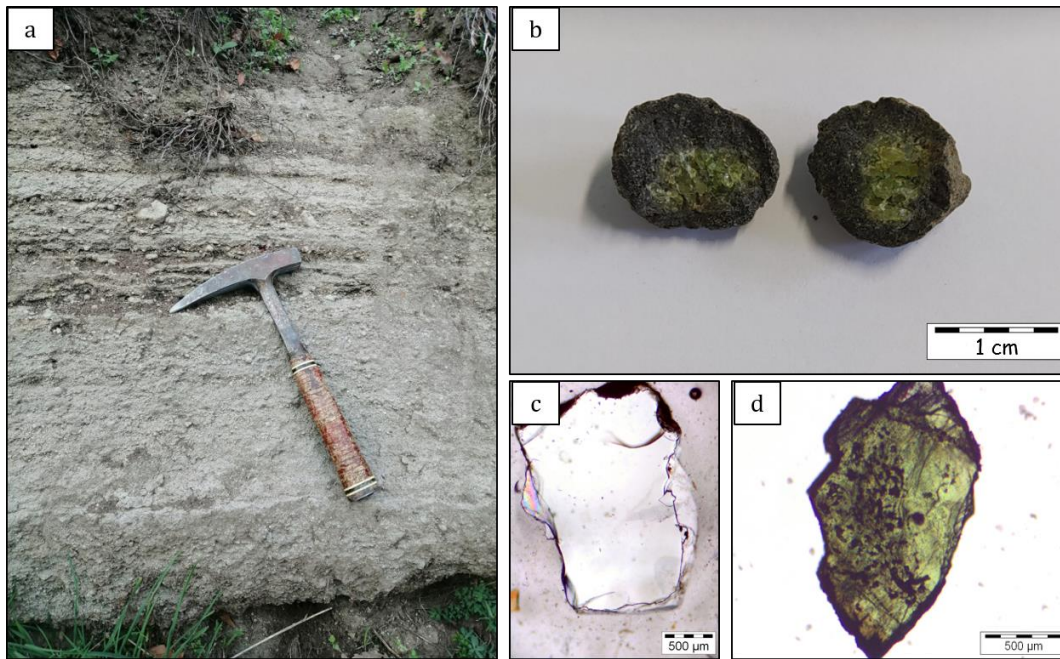
58 The Mt. Vulture volcano is a relatively small volcanic complex characterised by a central vent and
59 parasitic cones, domes, and lava plugs (Giannandrea et al., 2006). Its eruptive activity started at
60 730 ± 8 ka (Laurenzi et al., 1993) or 687 ± 8 ka (Villa & Buettner, 2009), and it continued until to
61 141 ± 11 ka (Villa & Buettner, 2009) with long inter-eruptive periods of quiescence ($> 10^5$ years,
62 Buettner et al., 2006). After the initial phase of volcanic activity, represented by pyroclastic
63 products with lava blocks and subordinate eccentric domes, the latest volcanic event was strongly
64 explosive, erupting melilitite-carbonatite tephra from maar-type craters (Stoppa & Principe, 1997).
65 These craters host two lakes (Monticchio Lakes) whose water dissolves mantle-derived volatiles
66 (Caracausi et al., 2009, 2013b), supporting the active degassing of mantle volatiles from this
67 volcano (Caracausi et al., 2009, 2015). The last volcanic activity (identified as Monticchio Lakes
68 Formation, Stoppa & Principe, 1997), fed by a melilitite-carbonatite magma, brought to the surface
69 some pelletal lapilli (enclosing abundant ultramafic mantle xenoliths and xenocrysts) considered
70 juvenile component of the melilititic-carbonatitic Monticchio diatreme and volatile component
71 (Lloyd & Stoppa, 2003). Thus, these products are particularly useful to characterize the mantle
72 source beneath Mt. Vulture, providing important information about the melilitite-carbonatite
73 magma and its mantle source.

74 Here we present the first detailed micro-thermometric analysis of fluid inclusions (FIs) hosted in
75 the ultramafic xenolith cores of pelletal lapilli and in loose olivine and clinopyroxene xenocrysts
76 from Mt. Vulture volcano (Monticchio Lakes Synthem, Lago Piccolo Sub-Synthem), in order to
77 describe the way which these very particular magmas are transported to the surface and the
78 possible implications in terms of volcanic hazard.

79 **2 Sample Description**

80 Were selected 29 pelletal lapilli set in a compact fine-grained carbonate-dominated matrix in the
81 ash-tuff phreatomagmatic deposit of Lago Piccolo Sub-Synthem, with the presence of ultramafic
82 xenoliths (dominantly wehrlitic) constituting the core of pelletal lapilli, surrounded by a variably
83 thick rim of micro-phenocrysts (Figures 1a and 1b). We also selected about 200 olivine and 100
84 emerald-green Cr-diopside loose xenocrysts (Figures 1c and 1d) from the fine-grained carbonate-
85 rich matrix, where loose xenocrysts of blackish clinopyroxene, amphibole, mica (phlogopite) and
86 spinel, were also present together with the pelletal lapilli. These loose xenocrysts are considered
87 as mantle debris from disaggregated nodules. In order to compare the fluid inclusions within the
88 loose olivine and Cr-diopside xenocrysts with the fluid inclusions within the ultramafic xenolith

89 cores of pelletal lapilli, we selected two representative wehrlite cores from the 29 pelletal lapilli,
 90 three olivines and two Cr-diopsides from the 200 and 100 loose xenocrysts respectively.



91 **Figure 1.** Sampling site and details on pelletal lapilli and loose crystals. a) Ash-rich tuff surge
 92 deposit of Lago Piccolo Sub-Synthem. b) Pelletal lapilli with ultramafic xenolith cores. c) Loose
 93 olivine xenocryst from the fine-grained matrix (parallel polars). d) Loose clinopyroxene (Cr-
 94 diopside) xenocryst from the fine-grained matrix (parallel polars).

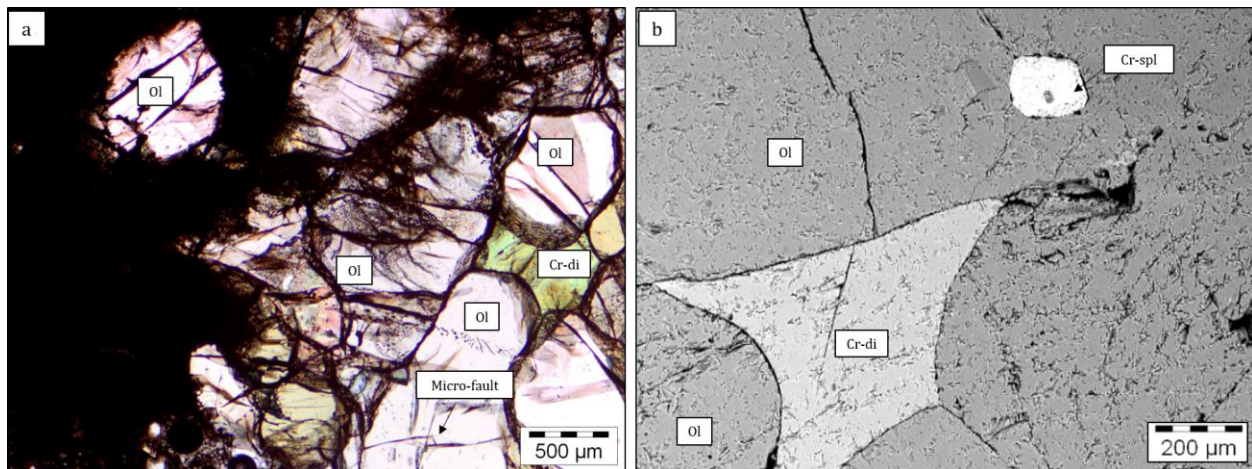
95 **3 Results**

96 The ultramafic xenolith cores of pelletal lapilli (the diameter of enclaves vary from 6 to 17 mm)
 97 are characterised by the presence of Mg-rich olivine (F_{090-91} , NiO varying from 0.35 to 0.38 wt.
 98 %, Table S1) and Cr-rich diopside (W_{046-48} , En_{47-48} , Fs_{4-5}) with relatively high Cr_2O_3 content (1.3-
 99 1.5 wt. %, Table S2). The grain size of the ultramafic xenolith cores is fine- to medium-grained
 100 (300-600 μm) with equigranular holocrystalline texture, granoblastic or interlocking with
 101 randomly oriented olivine and clinopyroxene variably elongated (Figures 2a and 2b). The variably
 102 thick rim of fine-grained material is composed essentially of häuyne micro-phenocrysts, with
 103 xenocrystic debris of olivine and clinopyroxene (Figure S1).

104 Loose (disaggregated) olivine xenocrysts show very similar composition (F_{089-92} , NiO = 0.37-0.41
 105 wt. %, Table S1) if compared with olivine from the ultramafic xenolith cores of pelletal lapilli. In
 106 the same way, almost all loose clinopyroxene xenocrysts show very similar composition (W_{046-48} ,
 107 En_{47-48} , Fs_{4-6} , Cr_2O_3 = 0.4-1.3 wt. %) if compared with clinopyroxene from the ultramafic xenolith
 108 cores of pelletal lapilli (Table S2). Thus, interestingly, the olivine and Cr-diopside minerals from
 109 the ultramafic xenoliths (wehrlites) and loose olivine and Cr-diopside xenocrysts, show almost the

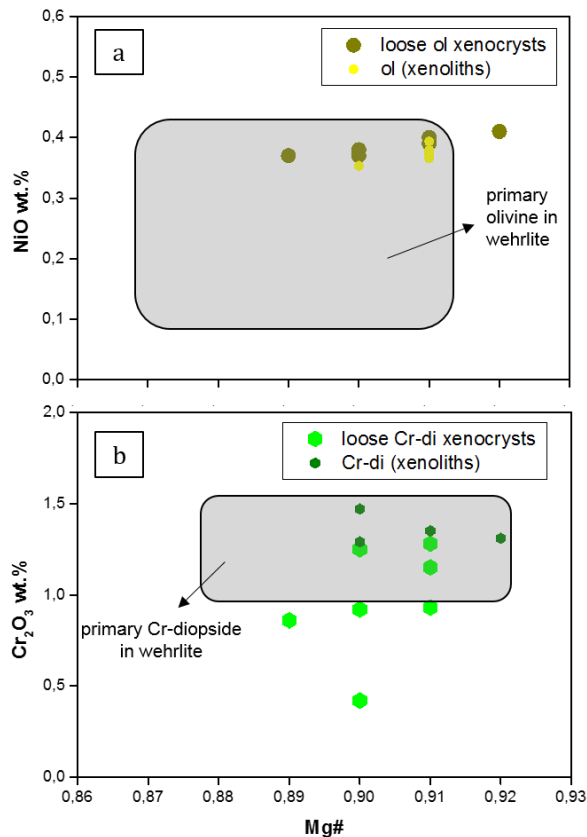
110 same minerochemical composition. Indeed, if plotted onto Mg# vs. NiO wt. % (olivine) and Cr₂O₃
 111 wt. % (Cr-diopside) diagrams, they show narrow ranges (Figures 3a and 3b).

112 All the studied fluid inclusions (FIs) are characterised by pure CO₂, with melting temperatures
 113 (T_m) ranging in a very narrow interval between -56.6 (*i.e.* the triple point of pure CO₂ at 1 bar)
 114 and -56.8 °C ± 0.1. FIs in loose olivine and Cr-diopside xenocrysts homogenized to liquid phase,
 115 with temperatures of homogenization (Th) ranging from 11.5 to 30.2 °C ($\rho = 0.58\text{-}0.85\text{ g/cm}^3$) and
 116 from -20.0 to 13.2 °C ($\rho = 0.84\text{-}1.03\text{ g/cm}^3$), respectively. FIs in the ultramafic cores of lapilli also
 117 homogenized to liquid phase, at Th ranging from -27.3 to -8.5 °C ($\rho = 0.98\text{-}1.06\text{ g/cm}^3$) in Cr-
 118 diopside crystals, and from -27.7 to -6.0 °C ($\rho = 0.96\text{-}1.07\text{ g/cm}^3$) in olivine crystals. Data of Th,
 119 densities, corrected densities and number of measures are reported in Table S3. The main
 120 geometric measurements of the aspect ratio and the internal structure of pelletal lapilli are reported
 121 in Table S4. Further details, also about analytical methods, are reported in Supporting Information
 122 S1.



123 **Figure 2.** Photomicrographs of the ultramafic core of pelletal lapilli from Vulture volcano. a) Sub-
 124 idioblastic texture with Cr-diopside (emerald green) and elongated olivine crystal with

125 intracrystalline deformations (parallel polars). b) BSE image showing Cr-diopside and olivine
 126 crystal with Cr-spinel inclusion.



127 **Figure 3.** Minerochemical composition of olivine and Cr-diopside from the ultramafic xenoliths
 128 (wehrlites) and loose olivine and Cr-diopside xenocrysts from Vulture volcano. a) Mg# vs. NiO
 129 wt. % in olivine crystals. b) Mg# vs. Cr₂O₃ wt. % in Cr-diopside crystals. The field of the
 130 primary olivine and Cr-diopside in wehrlite are from Jones et al. (2000).

131 **4 Significance of Fluid Inclusions Data**

132 In loose olivine and Cr-diopside xenocrysts FIAs are usually rounded or with a slight negative crystal
 133 shape (Figures 4a and 4b), and in some cases form trails of variable length lined in healed fractures
 134 (Figure 4c). As regards FIAs in the ultramafic cores of lapilli, they form fluid inclusions assemblages
 135 (FIAs) (Figure 4d), suggesting single events of entrapment.

136 The histograms of homogenization temperatures (Figure 5a) and densities (Figure 5b) essentially
 137 show a bimodal distribution, except in some cases where are almost unimodal, depending mainly
 138 on different trapping events of different products. The highest corrected density values of FIAs are
 139 in the olivine and Cr-diopside within the ultramafic cores of pelletal lapilli (1.10-1.11 g/cm³),
 140 corresponding to trapping pressures between 8.46 and 8.96 kbar (26-27 km). In the loose Cr-
 141 diopside xenocrysts trapping events occurred at 8.20-8.65 kbar (25-26 km) and at 6.72-7.22 kbar
 142 (21-22 km). Conversely, loose olivine xenocrysts show lower density values with a clear density

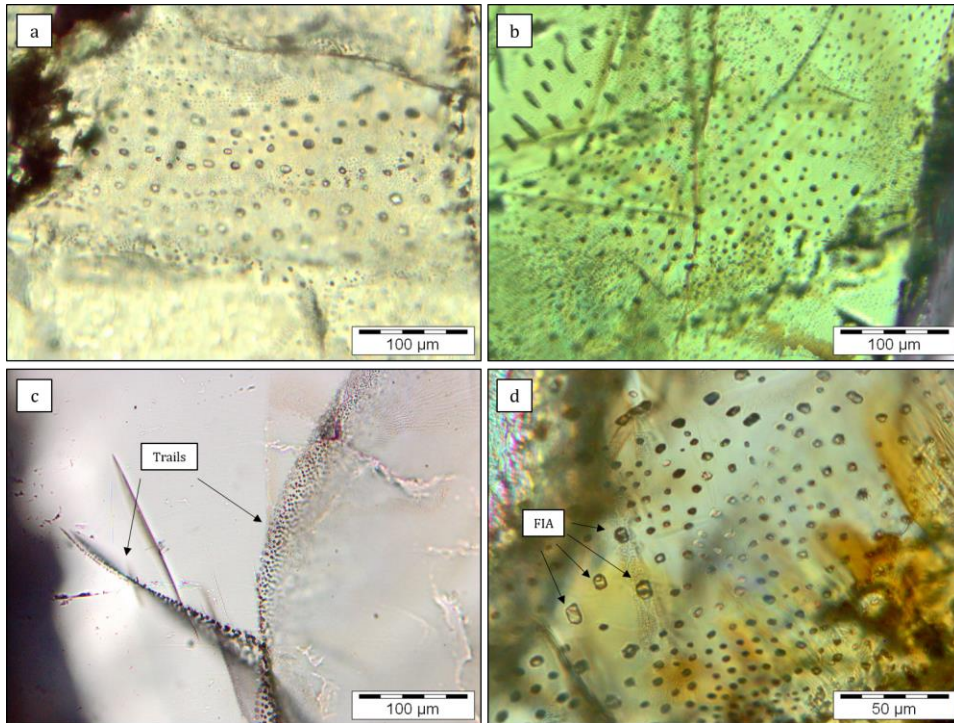
143 peak at 0.63 g/cm^3 and another at 0.75 g/cm^3 , with trapping pressures of 2.80-3.12 kbar (8-9 km)
144 and 4.05-4.49 kbar (12-13 km), respectively. The peak at 0.63 g/cm^3 is also slightly registered by
145 olivine within the ultramafic cores.

146 Combining textures, densities and relative distribution of FIs within the ultramafic cores of pelletal
147 lapilli and loose xenocrysts, it is possible to figure out the different fluid trapping events that
148 occurred during the transfer of the magmas from crust-mantle boundary to the surface. Olivine and
149 Cr-diopside within the ultramafic cores of pelletal lapilli, together with loose Cr-diopside
150 xenocrysts, register the first fluid trapping event at depths corresponding approximately to the
151 Moho beneath Mt. Vulture (about 32 km, Kelemework et al., 2021). Olivine composition (Fo %,
152 NiO), clinopyroxene Cr content and spinel Cr/Cr+Al, strongly suggest that the wehrlitic cores are
153 of mantle origin. Thus, wehrlitic cores of pelletal lapilli are not considered cumulates produced in
154 shallow level magma chambers and subsequently entrained by the erupting melilitite-carbonatite
155 magma during ascent to the surface (Beccaluva et al., 2002), but trapping pressures of FIs
156 constrained the wehrlitic cores of pelletal lapilli to a minimum depth of 26-27 km, near the crust-
157 mantle boundary. On the contrary, loose olivine xenocrysts record a different fluid trapping event
158 at much shallower depths, hosting late stage CO_2 -dominated fluids. It is therefore likely that
159 olivine and Cr-diopside within the ultramafic xenolith cores of pelletal lapilli and loose Cr-
160 diopside xenocrysts have different histories of fluid trapping events if compared with loose olivine
161 xenocrysts, although these latter show very similar minerochemical composition if compared with
162 olivine within the ultramafic xenolith cores of pelletal lapilli (see Table S1).

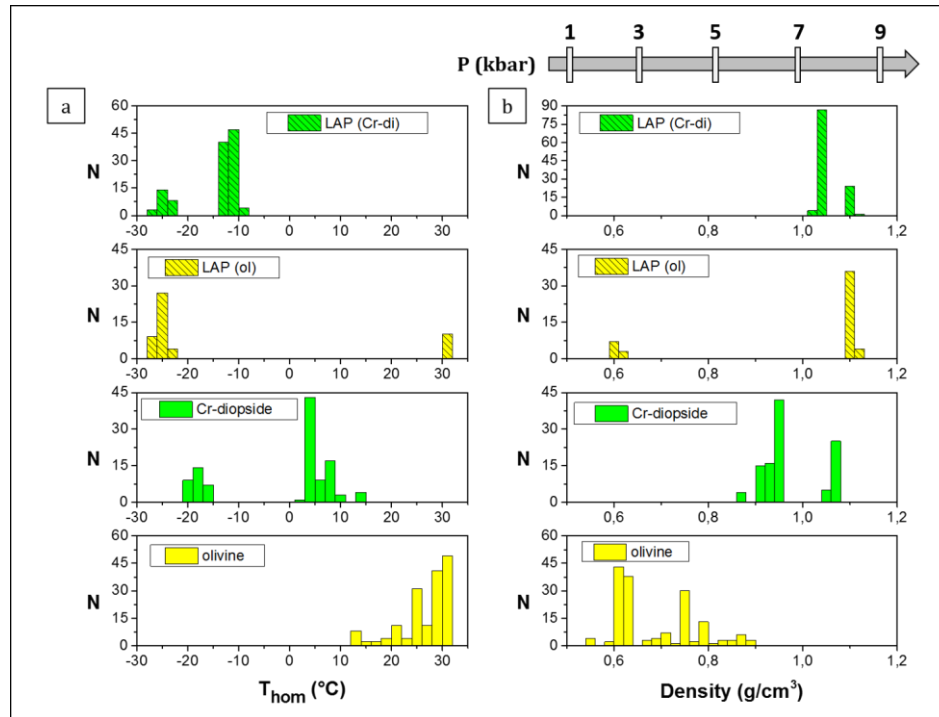
163 A continuous magma ascent translates in a density distribution of FIs with a single frequency
164 maximum at high-density values, and depending also on parameters such as the ascent velocity,
165 the original density should be recognizable as the upper limit of measured density values (Hanstee
166 & Klügel, 2008). On the contrary, if the magma experiences multibaric ponding stages, the density
167 distribution should show a multi-modal profile (*e.g.*, Zanon et al., 2003). Considering the very low
168 viscosity of a melilitite-carbonatite magma (*e.g.*, Stagno et al., 2020) and one of the basic
169 assumptions for the interpretation of FIs (*i.e.* that they have behaved as an isochoric system), it
170 seems that no fluid re-equilibrating event was registered by studied Mt. Vulture products, simply
171 showing different histories of fluid trapping events. Thus, we suggest that the melilitite-carbonatite

172 magma transported from Moho depth to the surface the ultramafic mantle xenoliths and Cr-
 173 diopside loose xenocrysts, while loose olivine xenocrysts were incorporated at shallower depths.

174 It is worthy of note that trapping pressures of volatiles in FIs from loose olivine xenocrysts (2.80-
 175 4.49 kbar, corresponding to depth of 8-13 km) overlap the depth (6-15 km) of a mafic body within
 176 the Vulture plumbing system (Improta et al., 2014), suggesting the occurrence of a magma
 177 stagnation and ponding level before eruption at this depth.



178 **Figure 4.** Thin section photomicrographs (parallel polars) of fluid inclusions and their
 179 arrangement. FIs within loose a) olivine and b) Cr-diopside xenocrysts. c) Intragranular trails of
 180 FIs in loose olivine xenocryst. (d) Fluid inclusions assemblage (FIA) in Cr-diopside from the
 181 ultramafic core of a pelletal lapillus.



182 **Figure 5.** Frequency distribution of a) homogenization temperatures and (b) densities of FIs hosted
 183 in loose olivine and Cr-diopside xenocrysts and in ultramafic cores of pelletal lapilli from Vulture
 184 volcano.

185 **5 Carbonatite Metasomatism and Magma Ascent Rate**

186 The study of mantle xenoliths represents a great tool to understand the composition and possible
 187 modification of a mantle source influenced by metasomatic fluids, especially in subduction zones.
 188 In this framework, the increase of modal clinopyroxene at the expense of orthopyroxene has been
 189 interpreted as a result of the interaction of ultramafic material with carbonatite melts, and
 190 carbonatite metasomatism is accompanied by the formation of secondary clinopyroxene formed
 191 during the reaction of carbonatite melts with orthopyroxene (the melt with the lowest SiO_2 activity
 192 dissolves the highest SiO_2 mantle mineral) (Dalton & Wood, 1993; Russell et al., 2012). Therefore,
 193 the process of “*wehrlitization*” is considered a consequence of carbonatite metasomatism in the
 194 lithospheric mantle.

195 Among the Mt. Vulture mantle products, the presence of wehrlite enclaves is widely recognized
 196 (e.g., Beccaluva et al., 2002; Downes et al., 2002; Jones et al., 2000) and is corroborated by our
 197 findings where pelletal lapilli cores are largely wehrlitic. Furthermore, according to Zong and Liu,
 198 (2018), specific crystallochemical patterns in clinopyroxenes (e.g., Mg# vs. Ca/Al; Ca/Al vs.
 199 $^{87}\text{Sr}/^{86}\text{Sr}$) fall into the mantle-related carbonate metasomatism field (Figure S2). Rosatelli et al.
 200 (2007) also suggest carbonatite melts as the main metasomatism agent of Mt. Vulture mantle
 201 source region, emphasizing the role of silicate-carbonatite magma immiscibility during the
 202 carbonated melt ascent to the surface (Solovova et al., 2005), this latter point supported by a
 203 number of experimental constrains underlying melilititic magma (the last erupted at Mt. Vulture)
 204 as the best candidate to exsolve an immiscible carbonatite melt (Brooker & Kjarsgaard, 2011).
 205 Further evidence of metasomatism by carbonatite-like melts is given by the presence of interstitial

206 calcite associated with Fe-Ni-sulfides between olivine grains in a mantle xenolith from Mt. Vulture
207 (Blanks et al., 2020).

208 Despite the last eruptive event of Mt. Vulture dates back to 141 ± 11 ka (Villa & Buettner, 2009),
209 geochemical evidences support that active magmatic degassing of mantle-derived volatiles is still
210 ongoing in Mt. Vulture area (Caracausi et al., 2009, 2013a), also showing how the relationship
211 between the deep CO₂ release and the time of its last eruption could be an important tool for
212 evaluating the state of current activity (Caracausi et al., 2015). Moreover, recent studies show how
213 the source of CO₂ degassing in Mt. Vulture area is related to the presence of a subcontinental
214 lithospheric mantle (SCLM), that sequesters large amounts of CO₂ due to the infiltration of fluids
215 and melts during carbonatite-like metasomatism (Bragagni et al., 2022). In this scenario the He
216 isotopic signature in fluid inclusions of the Vulture mantle xenoliths ($<6.1R_a$; R_a is the He isotopic
217 signature in air) overlap the range of the SCLM He end member (6.1 ± 0.9 ; Gautheron & Moreira,
218 2002).

219 Considering, 1) the active degassing of mantle-derived fluids in Mt. Vulture area (Caracausi et al.,
220 2009, 2015), 2) the explosive behaviour associated with a maar-diatreme system of the Monticchio
221 Lakes Synthem (MLS; Solovova et al., 2005; Stoppa & Principe, 1997), 3) the occurrence of small
222 amounts of magma at the Moho depth (< 1.6 %, Tumanian et al., 2012), in absence of mantle
223 upwelling or extensional tectonics that could favour decompression melting (Peccerillo &
224 Frezzotti, 2015), 4) the role of tectonics in the transfer of the mantle-derived magma and volatiles
225 and its control of the Vulture volcanism and outgassing (*e.g.*, Caracausi et al., 2013a; D'Orazio et
226 al., 2007; Rosenbaum et al., 2008), 5) the long inter-eruptive periods (> 140 ka, Buettner et al.,
227 2006) and 6) the recognized occurring of volatiles rich magmas at the mantle-crust boundary
228 (Section 4, Significance of Fluid Inclusions Data), we focused on modelling melilitite-carbonatite
229 magma ascent rate with its cargo of xenoliths and loose xenocrysts to the surface. In order to
230 constrain the ascent velocity of the melilitite-carbonatite magma, we used the equation from Lister
231 and Kerr (1991) and applied by Sparks et al. (2006) in their physical model.

232 Taking into consideration (i) a closed system during the magma ascent with a constant dike width
233 of 1 m, (ii) a magma density of 2500 kg/m^3 , (iii) a constant viscosity of 0.6 Pa s, and (iv) a mean
234 density of the crust of 2600 kg/m^3 , we obtain ascent rate of about 17 m/s (equation (8) from Sparks
235 et al. 2006), assuming that the buoyancy is the main driving force. Magma viscosity value is taken
236 from experimental studies of a representative melilitite synthetic melt (Stagno et al., 2020). Magma
237 density is calculated using the model of Ochs and Lange (1999) at 1100 °C and 10 kbar, assuming
238 a bulk composition from Stoppa and Principe (1997) with $\text{SiO}_2 = 37$ wt. %, and a mean CO₂ value
239 of 7.5 wt. %, obtained from the H₂O-CO₂ solubility model proposed by Moussallam et al. (2016).
240 Indeed, if we consider their model for a low SiO₂- and H₂O-free melts (our fluid inclusions study
241 indicates the presence of pure CO₂ as the main volatile phase, with no presence or very scarce of
242 H₂O), at about 30 km depth (crust-mantle boundary beneath Mt. Vulture area), we obtain CO₂
243 values between 5 and 10 wt. %. The model of Moussallam et al. (2016) is applied to a kimberlite
244 magmatism with $25 \text{ wt. \%} \leq \text{SiO}_2 \leq 32 \text{ wt. \%}$, and it is comparable to the melilitite-carbonatite
245 magmatism of Monticchio Lakes Syntheme with $\text{SiO}_2 < 40 \text{ wt. \%}$ (Stoppa & Principe, 1997).

246 Our result of the ascent rate of the melilitite-carbonatite magma is in the same order of the ascent
247 rates of kimberlite magmatism described by Moussallam et al. (2016). The direct effect of ascent
248 dynamics is that the melilitite-carbonatite magma could reach the surface from the depth of 30 km

249 in less than an hour. Considering also recent studies showing how volcanic systems where activity
250 has remained dormant for protracted periods (> 100 ka) still have the potential for reactivation
251 (Harangi et al., 2015a; Molnár et al., 2018, 2019), and in Mt. Vulture there is a possible link
252 between the development of tear faults, magmatism and related magma ascent along these tectonic
253 pathways (Peccerillo, 2017; Rosenbaum et al., 2008), our study supports that volcanic hazard in
254 melilitite-carbonatite volcanoes, even after long time of quiescence, should be carefully evaluated.

255 **6 Conclusion**

256 We analysed fluid inclusions (FIs) hosted in the wehrlitic cores of pelletal lapilli and in loose
257 xenocrysts of olivine and clinopyroxene brought to the surface by a melilitite-carbonatite magma
258 from the last eruption of Mt. Vulture volcano (Monticchio Lakes Synthème, Lago Piccolo Sub-
259 Synthém). We found CO₂-dominated FIs with different trapping pressures (from 2.80 to 8.96 kbar)
260 that correspond to magma storage at different depths within the volcano plumbing system (from 8
261 to 27 km). The deeper reservoir is close to the local Moho (32 km), while the shallower
262 corresponds to a solidified magmatic body imaged by geophysical investigations (Improta et al.,
263 2014). Modeling magma ascent rate results in quite high velocity for melilitite-carbonatite magma
264 from the crust-mantle boundary to the surface, in the order of 15-20 m/s. These evidences, coupled
265 to (i) the outgassing of magmatic volatiles at Mt. Vulture, which isotopic signature correspond to
266 those in the fluid inclusions of the last activity of the volcano (Caracausi et al., 2009, 2013a), and
267 to (ii) the presence of small amounts of melt ($< 1,6\%$) at the Moho depth, add constraints for
268 magma production and ascent pathways. Therefore, this study confirms that the scientific
269 community must pay attention also to the inactive volcanoes, because they could be still hazardous
270 systems notwithstanding the last volcanic activity occurred hundreds/thousands of years ago.

271 **Data Availability Statement**

272 The complete data set of minerochemical and micro-thermometric analyses of this study was
273 uploaded to the Zenodo FAIR aligned repository (www.zenodo.org) and will be available for
274 download at the required link: Carnevale et al. (2022). Micro-thermometry and minerochemical
275 composition of ultramafic xenoliths and minerals from Mt. Vulture volcano (southern Italy) [Data
276 set]. Zenodo. <https://doi.org/10.5281/zenodo.6426785>. Accessed 9 april 2022.

277 **Acknowledgments**

278 This study was partially funded by Fundação para a Ciência e Tecnologia, Portugal (MAGAT
279 project, ref. CIRCNA/OCT/0016/2019). The Instituto de Investigação em Vulcanologia e
280 Avaliação de Riscos (IVAR), Universidade dos Açores, is acknowledged for hosting GC and
281 providing access to analytical facilities. We are grateful to F. Langone for sampling of some
282 investigated pelletal lapilli, and to D. Mannetta for his contribution in samples preparation.

283 **References**

284 Beccaluva, L., Coltorti, M., Di Girolamo, P., Melluso, L., Milani, L., Morra, V., & Siena, F.
285 (2002). Petrogenesis and evolution of Mt. Vulture alkaline volcanism (Southern Italy).

- 286 *Mineralogy and Petrology*, 74(2–4), 277–297. <https://doi.org/10.1007/s007100200007>
- 287 Blanks, D. E., Holwell, D. A., Fiorentini, M. L., Moroni, M., Giuliani, A., Tassara, S., et al. (2020).
288 Fluxing of mantle carbon as a physical agent for metallogenic fertilization of the crust. *Nature*
289 *Communications*, 11(1). <https://doi.org/10.1038/s41467-020-18157-6>
- 290 Bouabdellah, M., Hoernle, K., Kchit, A., Duggen, S., Hauff, F., Klügel, A., et al. (2010).
291 Petrogenesis of the Eocene Tamazert continental carbonatites (Central High Atlas, Morocco):
292 Implications for a common source for the Tamazert and Canary and Cape Verde Island
293 carbonatites. *Journal of Petrology*, 51, 1655–1686. <https://doi.org/10.1093/petrology/egq033>
- 294 Bragagni, A., Mastroianni, F., Münker, C., Conticelli, S., & Avanzinelli, R. (2022). A carbon-rich
295 lithospheric mantle as a source for the large CO₂ emissions of Etna volcano (Italy). *Geology*,
296 50(4), 486–490. <https://doi.org/10.1130/g49510.1>
- 297 Brooker, R. A., & Kjarsgaard, B. A. (2011). Silicate-carbonate liquid immiscibility and phase
298 relations in the system SiO₂-Na₂O-Al₂O₃-CaO-CO₂ at 0.1-2.5 GPa with applications to
299 carbonatite genesis. *Journal of Petrology*, 52, 1281–1305.
300 <https://doi.org/10.1093/petrology/egq081>
- 301 Buettner, A., Principe, C., Villa, I. M., & Bocchini, D. (2006). Geochronologia ³⁹Ar-⁴⁰Ar del Monte
302 Vulture. In C. Principe (Ed.), *La Geologia del Monte Vulture* (pp. 73–86). Lavello.
- 303 Caracausi, A., Nuccio, P. M., Favara, R., Nicolosi, M., & Paternoster, M. (2009). Gas hazard
304 assessment at the Monticchio crater lakes of Mt. Vulture, a volcano in Southern Italy. *Terra*
305 *Nova*, 21(2), 83–87. <https://doi.org/10.1111/j.1365-3121.2008.00858.x>
- 306 Caracausi, A., Martelli, M., Nuccio, P. M., Paternoster, M., & Stuart, F. M. (2013a). Active
307 degassing of mantle-derived fluid: A geochemical study along the Vulture line, southern
308 Apennines (Italy). *Journal of Volcanology and Geothermal Research*, 253, 65–74.

- 309 <https://doi.org/10.1016/j.jvolgeores.2012.12.005>
- 310 Caracausi, A., Nicolosi, M., Nuccio, P. M., Favara, R., Paternoster, M., & Rosciglione, A. (2013b).
311 Geochemical insight into differences in the physical structures and dynamics of two adjacent
312 maar lakes at Mt. Vulture volcano (southern Italy). *Geochemistry, Geophysics, Geosystems*,
313 *14*(5), 1411–1434. <https://doi.org/10.1002/ggge.20111>
- 314 Caracausi, A., Paternoster, M., & Nuccio, P. M. (2015). Mantle CO₂ degassing at Mt. Vulture
315 volcano (Italy): Relationship between CO₂ outgassing of volcanoes and the time of their last
316 eruption. *Earth and Planetary Science Letters*, *411*, 268–280.
317 <https://doi.org/10.1016/j.epsl.2014.11.049>
- 318 Carnevale, G., Caracausi, A., Correale, A., Italiano, L., & Rotolo, S. G. (2021). An overview of
319 the geochemical characteristics of oceanic carbonatites: New insights from fuerteventura
320 carbonatites (Canary islands). *Minerals*, *11*(2). <https://doi.org/10.3390/min11020203>
- 321 Carnevale, G., Caracausi, A., Rotolo, S. G., Paternoster, M., & Zanon, V. (2022). Micro-
322 thermometry and minerochemical composition of ultramafic xenoliths and minerals from Mt.
323 Vulture volcano (southern Italy) [Data set]. Zenodo. <https://doi.org/10.5281/zenodo.6426785>
- 324 D’Orazio, M., Innocenti, F., Tonarini, S., & Doglioni, C. (2007). Carbonatites in a subduction
325 system: The Pleistocene alvikites from Mt. Vulture (southern Italy). *Lithos*, *98*(1–4), 313–
326 334. <https://doi.org/10.1016/j.lithos.2007.05.004>
- 327 Dalton, J. A., & Wood, B. J. (1993). The compositions of primary carbonate melts and their
328 evolution through wallrock reaction in the mantle. *Earth and Planetary Science Letters*, *119*,
329 511–525. [https://doi.org/10.1016/0012-821X\(93\)90059-I](https://doi.org/10.1016/0012-821X(93)90059-I)
- 330 Doucelance, R., Hammouda, T., Moreira, M., & Martins, J. C. (2010). Geochemical constraints
331 on depth of origin of oceanic carbonatites: The Cape Verde case. *Geochimica et*

- 332 *Cosmochimica Acta*, 74, 7261–7282. <https://doi.org/10.1016/j.gca.2010.09.024>
- 333 Downes, H., Kostoula, T., Jones, A. P., Beard, A. D., Thirlwall, M. F., & Bodinier, J. L. (2002).
334 Geochemistry and Sr-Nd isotopic compositions of mantle xenoliths from the Monte Vulture
335 carbonatite-melilitite volcano, central southern Italy. *Contributions to Mineralogy and*
336 *Petrology*, 144(1), 78–92. <https://doi.org/10.1007/s00410-002-0383-4>
- 337 Gautheron, C., & Moreira, M. (2002). Helium signature of the subcontinental lithospheric mantle.
338 *Earth and Planetary Science Letters*, 199, 39–47. [https://doi.org/10.1016/S0012-](https://doi.org/10.1016/S0012-821X(02)00563-0)
339 [821X\(02\)00563-0](https://doi.org/10.1016/S0012-821X(02)00563-0)
- 340 Giannandrea, P., La Volpe, L., Principe, C., & Schiattarella, M. (2006). Unità stratigrafiche a limiti
341 inconformi e storia evolutiva del vulcano medio-pleistocenico di Monte Vulture (Appennino
342 meridionale, Italia). *Bollettino Della Societa Geologica Italiana*, 125(1), 67–92.
- 343 Hansteen, T. H., & Klügel, A. (2008). Fluid inclusion thermobarometry as a tracer for magmatic
344 processes. *Reviews in Mineralogy and Geochemistry*, 69(Roedder 1984), 143–177.
345 <https://doi.org/10.2138/rmg.2008.69.5>
- 346 Harangi, S., Lukács, R., Schmitt, A. K., Dunkl, I., Molnár, K., Kiss, B., et al. (2015). Constraints
347 on the timing of Quaternary volcanism and duration of magma residence at Ciomadul
348 volcano, east-central Europe, from combined U-Th/He and U-Th zircon geochronology.
349 *Journal of Volcanology and Geothermal Research*, 301, 66–80.
350 <https://doi.org/10.1016/j.jvolgeores.2015.05.002>
- 351 Horton, F. (2021). Rapid recycling of subducted sedimentary carbon revealed by Afghanistan
352 carbonatite volcano. *Nature Geoscience*, 14(7), 508–512. [https://doi.org/10.1038/s41561-](https://doi.org/10.1038/s41561-021-00764-7)
353 [021-00764-7](https://doi.org/10.1038/s41561-021-00764-7)
- 354 Improta, L., De Gori, P., & Chiarabba, C. (2014). New insights into crustal structure, Cenozoic

- 355 magmatism, CO₂ degassing, and seismogenesis in the southern Apennines and Irpinia region
356 from local earthquake tomography. *Journal of Geophysical Research: Solid Earth*, 119(11),
357 8283–8311. <https://doi.org/10.1002/2013JB010890>
- 358 Jones, A. P., Kostoula, T., Stoppa, F., & Woolley, A. R. (2000). Petrography and mineral chemistry
359 of mantle xenoliths in a carbonate-rich melilititic tuff from Mt. Vulture volcano, southern
360 Italy. *Mineralogical Magazine*, 64(4), 593–613. <https://doi.org/10.1180/002646100549634>
- 361 Jones, A. P., Genge, M., & Carmody, L. (2013). Carbonate melts and carbonatites. *Reviews in*
362 *Mineralogy and Geochemistry*, 75, 289–322. <https://doi.org/10.2138/rmg.2013.75.10>
- 363 Kelemework, Y., Milano, M., La Manna, M., de Alteriis, G., Iorio, M., & Fedi, M. (2021). Crustal
364 structure in the Campanian region (Southern Apennines, Italy) from potential field modelling.
365 *Scientific Reports*, 11(1), 1–18. <https://doi.org/10.1038/s41598-021-93945-8>
- 366 Laurenzi, M.A., Brocchini, D., Principe, C., & Ferrara, G. (1993). Mt. Vulture volcano
367 chronostratigraphy and the effectiveness of dating young phlogopites. Abstracts EUG 7,
368 Strasburgo, 572-573.
- 369 Li, Y., Zhang, J., Mostofa, K. M. G., Wang, Y., Yu, S., Cai, Z., et al. (2018). Petrogenesis of
370 carbonatites in the Luliangshan region, North Qaidam, northern Tibet, China: Evidence for
371 recycling of sedimentary carbonate and mantle metasomatism within a subduction zone.
372 *Lithos*, 322, 148–165. <https://doi.org/10.1016/j.lithos.2018.10.010>
- 373 Lister, J. R., & Kerr, R. C. (1991). Fluid-mechanical models of crack propagation and their
374 application to magma transport in dykes. *Journal of Geophysical Research*, 96(B6), 49–77.
375 <https://doi.org/10.1029/91jb00600>
- 376 Lloyd, F. E., & Stoppa, F. (2003). Pelletal Lapilli in Diatremes – Some Inspiration from the Old
377 Masters. *GeoLines*, 15, 65–71.

- 378 Mata, J., Moreira, M., Doucelance, R., Ader, M., & Silva, L. C. (2010). Noble gas and carbon
379 isotopic signatures of Cape Verde oceanic carbonatites: Implications for carbon provenance.
380 *Earth and Planetary Science Letters*, 291, 70–83. <https://doi.org/10.1016/j.epsl.2009.12.052>
- 381 Molnár, K., Harangi, S., Lukács, R., Dunkl, I., Schmitt, A. K., Kiss, B., et al. (2018). The onset of
382 the volcanism in the Ciomadul Volcanic Dome Complex (Eastern Carpathians): Eruption
383 chronology and magma type variation. *Journal of Volcanology and Geothermal Research*,
384 354, 39–56. <https://doi.org/10.1016/j.jvolgeores.2018.01.025>
- 385 Molnár, K., Lukács, R., Dunkl, I., Schmitt, A. K., Kiss, B., Seghedi, I., et al. (2019). Episodes of
386 dormancy and eruption of the Late Pleistocene Ciomadul volcanic complex (Eastern
387 Carpathians, Romania) constrained by zircon geochronology. *Journal of Volcanology and*
388 *Geothermal Research*, 373, 133–147. <https://doi.org/10.1016/j.jvolgeores.2019.01.025>
- 389 Moussallam, Y., Morizet, Y., & Gaillard, F. (2016). H₂O–CO₂ solubility in low SiO₂-melts and
390 the unique mode of kimberlite degassing and emplacement. *Earth and Planetary Science*
391 *Letters*, 447, 151–160. <https://doi.org/10.1016/j.epsl.2016.04.037>
- 392 Ochs, F. A., & Lange, R. A. (1999). The density of hydrous magmatic liquids. *Science*, 283(5406),
393 1314–1317. <https://doi.org/10.1126/science.283.5406.1314>
- 394 Peccerillo, A., & Frezzotti, M. L. (2015). Magmatism, mantle evolution and geodynamics at the
395 converging plate margins of Italy. *Journal of the Geological Society*, 172(4), 407–427.
396 <https://doi.org/10.1144/jgs2014-085>
- 397 Peccerillo, A.. (2017). The Apulian Province (Mount Vulture). *Advances in Volcanology*, 203–
398 216. https://doi.org/10.1007/978-3-319-42491-0_8
- 399 Rosatelli, G., Wall, F., & Stoppa, F. (2007). Calcio-carbonatite melts and metasomatism in the
400 mantle beneath Mt. Vulture (Southern Italy). *Lithos*, 99(3–4), 229–248.

- 401 <https://doi.org/10.1016/j.lithos.2007.05.011>
- 402 Rosenbaum, G., Gasparon, M., Lucente, F. P., Peccerillo, A., & Miller, M. S. (2008). Kinematics
403 of slab tear faults during subduction segmentation and implications for Italian magmatism.
404 *Tectonics*, 27(2), 1–16. <https://doi.org/10.1029/2007TC002143>
- 405 Russell, J. K., Porritt, L. A., Lavallé, Y., & Dingwell, D. B. (2012). Kimberlite ascent by
406 assimilation-fuelled buoyancy. *Nature*, 481(7381), 352–356.
407 <https://doi.org/10.1038/nature10740>
- 408 Schmidt, M. W., & Weidendorfer, D. (2018). Carbonatites in oceanic hotspots. *Geology*, 46, 435–
409 438. <https://doi.org/10.1130/G39621.1>
- 410 Solovova, I. P., Girnis, A. V., Kogarko, L. N., Kononkova, N. N., Stoppa, F., & Rosatelli, G.
411 (2005). Compositions of magmas and carbonate-silicate liquid immiscibility in the Vulture
412 alkaline igneous complex, Italy. *Lithos*, 85(1-4 SPEC. ISS.), 113–128.
413 <https://doi.org/10.1016/j.lithos.2005.03.022>
- 414 Sparks, R. S. J., Baker, L., Brown, R. J., Field, M., Schumacher, J., Stripp, G., & Walters, A.
415 (2006). Dynamical constraints on kimberlite volcanism. *Journal of Volcanology and*
416 *Geothermal Research*, 155(1–2), 18–48. <https://doi.org/10.1016/j.jvolgeores.2006.02.010>
- 417 Stagno, V., Stopponi, V., Kono, Y., D’arco, A., Lupi, S., Romano, C., et al. (2020). The viscosity
418 and atomic structure of volatile-bearing melilititic melts at high pressure and temperature and
419 the transport of deep carbon. *Minerals*, 10(3), 1–13. <https://doi.org/10.3390/min10030267>
- 420 Stoppa, F., & Principe, C. (1997). Eruption style and petrology of a new carbonatitic suite from
421 the Mt. Vulture Southern Italy /: The Monticchio Lakes Formation. *Journal of Volcanology*
422 *and Geothermal Research*, 78(3–4), 251–265. [https://doi.org/10.1016/S0377-](https://doi.org/10.1016/S0377-0273(97)00004-8)
423 [0273\(97\)00004-8](https://doi.org/10.1016/S0377-0273(97)00004-8)

- 424 Tumanian, M., Frezzotti, M. L., Peccerillo, A., Brandmayr, E., & Panza, G. F. (2012). Thermal
425 structure of the shallow upper mantle beneath Italy and neighbouring areas: Correlation with
426 magmatic activity and geodynamic significance. *Earth-Science Reviews*, *114*(3–4), 369–385.
427 <https://doi.org/10.1016/j.earscirev.2012.07.002>
- 428 Verplanck, P. L., Mariano, A. N., & Mariano, A. (2019). Rare Earth Element Ore Geology of
429 Carbonatites. *Rare Earth and Critical Elements in Ore Deposits*, 5–32.
430 <https://doi.org/10.5382/rev.18.01>
- 431 Villa, I. M., & Buettner, A. (2009). Chronostratigraphy of Monte Vulture volcano (southern Italy):
432 Secondary mineral microtextures and ^{39}Ar - ^{40}Ar systematics. *Bulletin of Volcanology*, *71*(10),
433 1195–1208. <https://doi.org/10.1007/s00445-009-0294-6>
- 434 Woolley, A. R., & Kjarsgaard, B. A. (2008). Carbonatite occurrences of the world: map and
435 database. *Geological Survey of Canada*, *5796*, 1–28.
436 <https://doi.org/https://doi.org/10.4095/225115>
- 437 Zanon, V., Frezzotti, M.-L., & Peccerillo, A. (2003). Magmatic feeding system and crustal magma
438 accumulation beneath Vulcano Island (Italy): Evidence from CO_2 fluid inclusions in quartz
439 xenoliths . *Journal of Geophysical Research: Solid Earth*, *108*(B6).
440 <https://doi.org/10.1029/2002jb002140>
- 441 Zong, K., & Liu, Y. (2018). Carbonate metasomatism in the lithospheric mantle: Implications for
442 cratonic destruction in North China. *Science China Earth Sciences*, *61*(6), 711–729.
443 <https://doi.org/10.1007/s11430-017-9185-2>

444 **References From the Supporting Information**

- 445 Bakker, R. J. (2003). Package FLUIDS 1. Computer programs for analysis of fluid inclusion data
446 and for modelling bulk fluid properties. *Chemical Geology*, 194(1–3), 3–23.
447 [https://doi.org/10.1016/S0009-2541\(02\)00268-1](https://doi.org/10.1016/S0009-2541(02)00268-1)
- 448 D’Orazio, M., Innocenti, F., Tonarini, S., & Doglioni, C. (2008). Reply to the discussion of:
449 “Carbonatites in a subduction system: The Pleistocene alvikites from Mt. Vulture (Southern
450 Italy)” by M. D’Orazio, F. Innocenti, S. Tonarini and C. Doglioni (*Lithos* 98, 313-334) by F.
451 Stoppa, C. Principe and P. Giannandrea. *Lithos*, 103(3–4), 557–561.
452 <https://doi.org/10.1016/j.lithos.2007.10.010>
- 453 Gernon, T. M., Brown, R. J., Tait, M. A., & Hincks, T. K. (2012). The origin of pelletal lapilli in
454 explosive kimberlite eruptions. *Nature Communications*, 3, 832–837.
455 <https://doi.org/10.1038/ncomms1842>
- 456 Scrocca, D., Sciamanna, S., Di Luzio, E., Tozzi, M., Nicolai, C., & Gambini, R. (2007). Structural
457 setting along the CROP-04 deep seismic profile (Southern Apennines - Italy). *Bollettino*
458 *Della Società Geologica Italiana*, Supplemento, 7, 283–296.
- 459 Sterner, S. M., & Bodnar, R. J. (1991). Synthetic fluid inclusions. X: Experimental determination
460 of P-V-T-X properties in the CO₂-H₂O system to 6 kb and 700 °C. *American Journal of*
461 *Science*, 291, 1–54. <https://doi.org/https://doi.org/10.2475/ajs.291.1.1>
- 462 Stoppa, F., Principe, C., & Giannandrea, P. (2008). Comments on: Carbonatites in a subduction
463 system: The Pleistocene alvikites from Mt. Vulture (southern Italy) by d’Orazio et al., (2007).
464 *Lithos*, 103(3–4), 550–556. <https://doi.org/10.1016/j.lithos.2007.10.012>